ChemSusChem

Supporting Information

# SiCO Ceramics as Storage Materials for Alkali Metals/Ions: Insights on Structure Moieties from Solid-State NMR and DFT Calculations

Edina Šić, Jochen Rohrer,* Emmanuel III Ricohermoso, Karsten Albe, Emmanuel Ionescu, Ralf Riedel, Hergen Breitzke, Torsten Gutmann,* and Gerd Buntkowsky*This publication is part of a joint Special Collection of ChemSusChem, Batteries & Supercaps, and Energy Technology including invited contributions focusing on the “International Conference on Sodium Batteries (ICNaB)”. Please visit  to view all contributions.

***Elemental Analysis***

The elemental composition of each sample was determined via the hot gas extraction method. A carbon analyzer (CS 800, Eltra GmbH, Neuss, Germany) was used to measure the content of carbon by detecting and quantifying the oxidized carbon species using IR spectroscopy. The oxygen content was quantified using a nitrogen/oxygen analyzer (Leco TC-436, Leco Corporation, Michigan, US).

Table S1. Elemental composition of the synthesized PDC-s with varying carbon content.

| | Volume in % | | | Element Content in wt % | | |
|---|---|---|---|---|---|---|
| sample | $SiO_2$ | SiC | Free Carbon | Si | O | C |
| SiCO-C14% | 76.75 | 12.24 | 11.01 | 46.65 | 39.4 | 13.95 |
| SiCO-C24% | 54.49 | 27.83 | 17.68 | 49.13 | 26.44 | 24.43 |
| SiCO-C36% | 51.19 | 11.66 | 36.43 | 36.53 | 27.9 | 35.57 |
| SiCO-C55% | 30.19 | 12.28 | 57.53 | 27.96 | 16.93 | 55.11 |

***Results of NMR deconvolution***

Table S2. Fit data for the Hahn-echo $^{29}Si$ MAS NMR spectra of the SiOC-PDCs with carbon content between 14-55 % shown in the manuscript in Figure 3b).

| | | Si-species | | | |
|---|---|---|---|---|---|
| sample | shift/width | $SiO_4$ | $SiCO_3$ | $SiC_2O_2$ | $SiC_4$ |
| SiCO-C14% | δ (ppm) | -104.5 | -73 | -40 | - |
| | fwhm (ppm) | 22 | 22 | 33 | - |
| SiCO-C24% | δ (ppm) | -99.55 | -68.84 | -36.37 | -17 |
| | fwhm (ppm) | 17 | 27.56 | 24.8 | 15.5 |
| SiCO-C36% | δ (ppm) | -106 | -75 | -37.12 | - |
| | fwhm (ppm) | 24 | 28.8 | 25.48 | - |
| SiCO-C55% | δ (ppm) | -99 | -71 | -39 | -18 |
| | fwhm (ppm) | 24 | 26 | 34 | 15 |

Table S3. The semi-quantitative estimation of the $SiC_xO_{4-x}$-fractions achieved applying the line deconvolution of the Hahn-echo $^{29}Si$ MAS NMR data of the SiOC-PDCs presented in the manuscript in Figure 3b).

| Si-species in % | | | | |
|---|---|---|---|---|
| sample | $SiO_4$ | $SiCO_3$ | $SiC_2O_2$ | $SiC_4$ |
| SiCO-C14% | 51 | 38 | 11 | - |
| SiCO-C24% | 15 | 40 | 34 | 11 |
| SiCO-C36% | 68 | 28 | 4 | - |
| SiCO-C55% | 21 | 35 | 39 | 5 |

Table S4. Fit data for the $^{29}Si$ CPMAS NMR spectra of the SiOC-PDCs with carbon content between 14-55 % provided in the manuscript in Figure 3c).

| sample | shift/width | Si-species | | | | |
|---|---|---|---|---|---|---|
| | | $SiO_4$ | $SiCO_3$ | $SiC_2O_2$ | $SiC_4$ | $SiC_3O$ |
| SiCO-C14% | δ (ppm) | -109.68 | -71.60 | -31.90 | -16 | -7.3 |
| | fwhm (ppm) | 20.66 | 22 | 21 | 43 | 19 |
| SiCO-C24% | δ (ppm) | -106.5 | -71.9 | -34.06 | -17.5 | -7.8 |
| | fwhm (ppm) | 29 | 23 | 23 | 45 | 23 |
| SiCO-C36% | δ (ppm) | -104.06 | -74.40 | -38.70 | -16.62 | -5 |
| | fwhm (ppm) | 28.49 | 26.42 | 23.71 | 26.63 | 30.30 |
| SiCO-C55% | δ (ppm) | -102.64 | -70.91 | -35.74 | -17.83 | -7.06 |
| | fwhm (ppm) | 28.96 | 23.8 | 21.99 | 48.59 | 17.64 |

Table S5. Percentages of the $SiC_xO_{4-x}$-fractions extracted from the $^{29}Si$ CPMAS NMR spectra of the SiOC-PDCs in Figure 3c).

| Si-species in % | | | | | |
|---|---|---|---|---|---|
| sample | $SiO_4$ | $SiCO_3$ | $SiC_2O_2$ | $SiC_4$ | $SiC_3O$ |
| SiCO-C14% | 25 | 44 | 16 | 5 | 10 |
| SiCO-C24% | 17 | 28 | 23 | 6 | 25 |
| SiCO-C36% | 34 | 26 | 14 | 22 | 4 |
| SiCO-C55% | 19 | 25 | 9 | 42 | 5 |

| Table S6. Fit data for the Hahn-echo $^{13}C$ MAS NMR spectra of the SiOC-PDCs with different carbon content shown in the manuscript in Figure 4b). | | | | |
|---|---|---|---|---|
| sample | shift/width | C-species | | |
| | | $C_{sp2}$ | $C_{sp2}$ | $C_{sp3}$ |
| SiCO-C14% | δ (ppm) | 139.28 | - | 23.84 |
| | fwhm (ppm) | 76.21 | - | 83.40 |
| SiCO-C24% | δ (ppm) | 137.6 | 127.46 | 23.51 |
| | fwhm (ppm) | 107.31 | 31.29 | 47.7 |
| SiCO-C36% | δ (ppm) | 122.32 | 118.43 | - |
| | fwhm (ppm) | 28.24 | 90.16 | - |
| SiCO-C55% | δ (ppm) | 130.66 | 121.17 | - |
| | fwhm (ppm) | 82.13 | 25.63 | - |

| Table S7. Percentages of the C-fractions achieved from the Hahn-echo $^{13}C$ MAS NMR spectra of the SiOC-PDCs in Figure 4b). | | | |
|---|---|---|---|
| C-species in % | | | |
| sample | $C_{sp2}$ | $C_{sp2}$ | $C_{sp3}$ |
| SiCO-C14% | 52 | - | 48 |
| SiCO-C24% | 35 | 19 | 46 |
| SiCO-C36% | 6 | 94 | - |
| SiCO-C55% | 87 | 13 | - |

| Table S8. Fit data for the $^{13}C$ CPMAS NMR spectra of the SiOC-PDCs with different carbon content shown in the manuscript in Figure 4c). | | | | | |
|---|---|---|---|---|---|
| sample | shift/width | C-species | | | |
| | | CO-group | $C_{sp2}$ | $CSi_4$ | $SiC_xO_{4-x}$ |
| SiCO-C14% | δ (ppm) | 176.08 | 139.66 | 15.02 | -13.31 |
| | fwhm (ppm) | 15 | 29.50 | 32.8 | 42.47 |
| SiCO-C24% | δ (ppm) | 175.09 | 138.9 | 14.88 | -12.85 |
| | fwhm (ppm) | 15.25 | 32 | 32 | 57.07 |
| SiCO-C36% | δ (ppm) | 173.7 | 130.4 | 14.45 | -10.65 |
| | fwhm (ppm) | 12.26 | 39 | 32.44 | 50.54 |
| SiCO-C55% | δ (ppm) | 174.9 | 131.06 | 15.34 | -13.58 |
| | fwhm (ppm) | 17.91 | 32.72 | 32.31 | 30.92 |

| Table S9. Percentages of the C-fractions obtained from the $^{13}C$ CPMAS NMR spectra of the SiOC-PDCs in Figure 4c). | | | | |
|---|---|---|---|---|
| C-species in % | | | | |
| sample | CO-group | $C_{sp2}$ | $CSi_4$ | $SiC_xO_{4-x}$ |
| SiCO-C14% | 31 | 28 | 26 | 15 |
| SiCO-C24% | 29 | 27 | 29 | 15 |
| SiCO-C36% | 14 | 47 | 13 | 26 |
| SiCO-C55% | 20 | 56 | 14 | 10 |

***Additional NMR spectra***

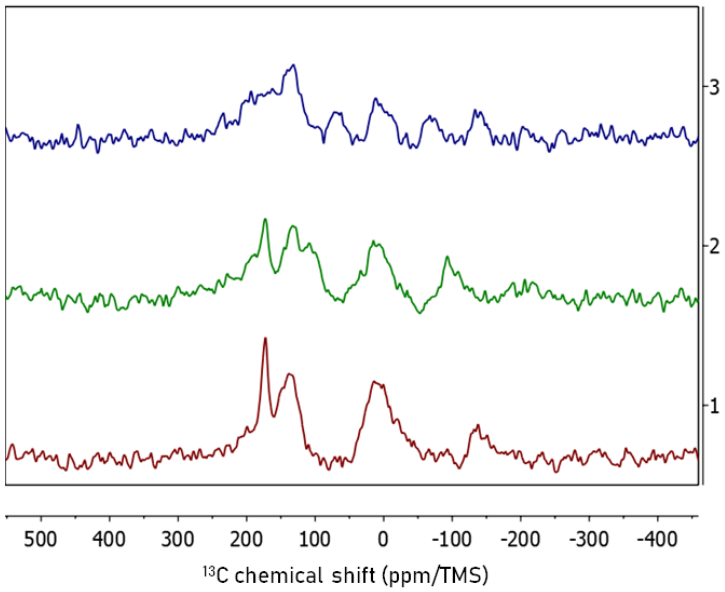


Figure S1. $^{13}C$ CPMAS NMR spectra of SiCO-C14% collected at 7 T applying the different spinning frequencies of 1) 10 kHz 2) 7 kHz and 3) 5 kHz to inspect the isotropic chemical behavior of the signal at 175 ppm.

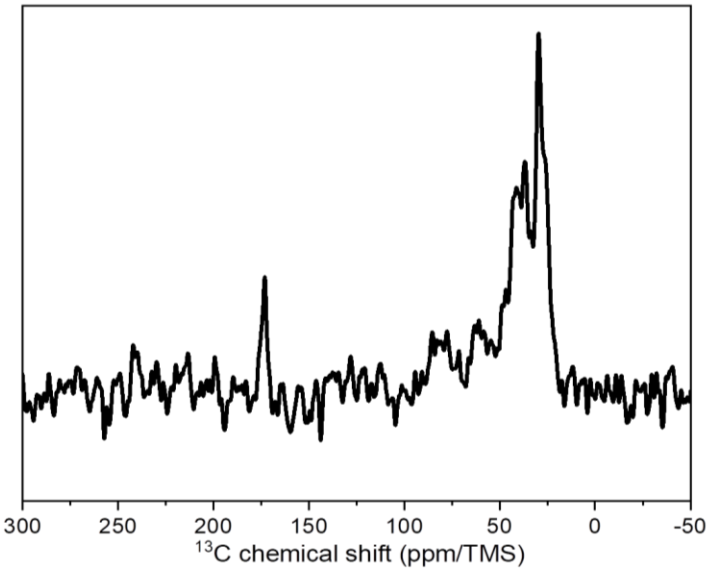


Figure S2. $^{13}C$ CPMAS NMR spectra of SiCO-C14% achieved at 14.1 T and 10 kHz.

***Atomistic modelling***

***Molecular dynamics simulations***

Molecular-dynamics (MD) cook-and-quench simulations were performed using LAMMPS [1] in order to prepare amorphous silica and carbon models; the silica models were then used as host matrix for further embedding of C and further optimized using density functional theory calculations (details see below). In all MD simulations an Nose-Hoover thermostat [2,3] and a Parrinello-Rahman barostat [4] was used to control temperature and pressure. A time step of 1 fs, and damping factors of 100 fs (thermostat) and 1000 fs (barostat) were used. For silica, we used the recent Gaussian Approximation Potential (GAP) of Erhard et al. [5], which is capable to generate ideal networks by simple melt quenching. Initially a crystalline structure consisting of 192 atoms was heated to 3000 K, then quenched back to 300 K and finally relaxed at zero K. Four-fold coordinated carbon was now introduced by (i) replacing a Si atom in the silica network with C, (ii) removing all neighboring O, and (iii) displacing all $2^{nd}$ nearest-neighbor Si atoms towards the inserted C. Thereafter density functional theory (DFT) relaxation are performed for further optimization (computational details, see below). We emphasize that these DFT relaxations must be performed with care to preserve the ideal 4-fold coordination of C and/or Si in the vicinity of

the inserted C. After several attempts we found that compression of the initial (carbonized) structure and slowly releasing the stress (by iteratively increasing the volume isotropically in between atomic relaxations) significantly helps to avoid breaking of bonds during optimization. Eventually (after four to five iterations), a full optimization of the model (keeping the orthogonality of the cell vectors) is performed. Despite this careful construction, still, some of the C-Si bonds break during the relaxation processes, eventually leading to the occurrence of minor defects. Chemical shifts associated with atoms inside such defective environments are not further reported here.

For the disordered carbon model, a classical interatomic potential [6] was used. Various replicas were considered. Each replica consisted of randomly distributed C chains and rings. In more detail, lignin fragments [7], with all non-carbon atoms stripped off were distributed on a regular grid and rotated randomly. The system was heated to 1000 K, then quenched back to 300 K and finally relaxed at zero K. The lowest-energy structure among all replicas was further optimized using DFT calculations. This configuration consists of 72% 3-fold, 23% 4-fold, and 5% 2-fold coordinated carbon.

***Electronic structure calculations***

The electronic-structure calculations were performed using the projector-augmented plane wave DFT codes GPAW (for optimization) and VASP (for calculating chemical shifts) [8–11]. In both cases, the PBE [12] implementation of the generalized-gradient approximation was used. For all DFT calculations, the energy cut-off was set to 800 eV. Brillouin-zone samplings [13] are listed in Table 1 together with cell dimensions and corresponding k-point densities. We have verified that the calculated chemical shifts are converged within +/- 1 ppm.

| Table S10. Lattice parameters, Monkhorst-Pack k-point meshes, and corresponding k-point densities $n_k = N_k * a_k$ for all considered systems. For SiCO, various compositions were considered; we thus give the average lattice parameters. | | | | | | | | | |
|---|---|---|---|---|---|---|---|---|---|
| System | Lattice parameters (Å) | | | # of k points | | | K-point density (Å) | | |
| | $a_1$ | $a_2$ | $a_3$ | $N_1$ | $N_2$ | $N_3$ | $n_1$ | $n_2$ | $n_3$ |
| SiOC | 13.353 | 13.220 | 13.419 | 1 | 1 | 1 | 13 | 13 | 13 |
| d-C | 14.526 | 9.544 | 8.430 | 1 | 2 | 2 | 14.5 | 19 | 17 |
| TMS | 15.000 | 15.000 | 15.000 | 1 | 1 | 1 | 15 | 15 | 15 |

**Chemical shifts**

The Tables S11 and S12 summarize the calculated chemical shifts of Si and C in different chemical environments. This data forms the basis of the histograms presented in Figure 2 in the main text.

| Table S11. Calculated chemical shifts and standard deviations in ppm for Si in different environments. The degeneracy reflects the number of atoms in a particular bonding environment present in all model systems. | | | | |
|---|---|---|---|---|
| Bond. Env. | degeneracy | Relative to $SiO_4$ | Relative to TMS | stdev |
| $SiO_4$ | 1070 | 0 | -103 | 11 |
| $SiCO_3$ | 161 | + 33 | -70 | 15 |
| $SiC_2O_2$ | 32 | + 64 | -39 | 10 |
| $SiC_3O$ | 9 | + 100 | -3 | 16 |
| $SiC_4$ | 6 | + 93 | -10 | 8 |

| Table S12. Calculated chemical shifts and standard deviations in ppm for C in different environments. | | | | |
|---|---|---|---|---|
| Bond. Env. | degeneracy | Relative to SiC (zincblende) | Relative to TMS ($Si(CH_3)_4$) | stdev |
| $CSi_4$ | 47 | 39 | 80 | 18 |
| $CSi_2H_2$ | 8 | -25 | 16 | 2 |
| $CC_3$ | 98 | 112 | 153 | 18 |

| | | | | |
|---|---|---|---|---|
| $CC_4$ | 31 | 50 | 91 | 15 |
| $CSi_3$ | 98 | 36 | 77 | 38 |
| $CC_2$ | 7 | 155 | 196 | 43 |

## References


[1] A.P. Thompson, H.M. Aktulga, R. Berger, D.S. Bolintineanu, W.M. Brown, P.S. Crozier, P.J. in 't Veld, A. Kohlmeyer, S.G. Moore, T.D. Nguyen, R. Shan, M.J. Stevens, J. Tranchida, C. Trott, S.J. Plimpton, LAMMPS - a flexible simulation tool for particle-based materials modeling at the atomic, meso, and continuum scales, Computer Physics Communications 271 (2022) 108171. https://doi.org/10.1016/j.cpc.2021.108171.

[2] W.G. Hoover, Canonical dynamics: Equilibrium phase-space distributions.

[3] S. Nosé, A unified formulation of the constant temperature molecular dynamics methods, J. Chem. Phys. 81 (1984) 511–519. https://doi.org/10.1063/1.447334.

[4] M. Parrinello, A. Rahman, Polymorphic transitions in single crystals: A new molecular dynamics method, Journal of Applied Physics 52 (1981) 7182–7190. https://doi.org/10.1063/1.328693.

[5] L.C. Erhard, J. Rohrer, K. Albe, V.L. Deringer, A machine-learned interatomic potential for silica and its relation to empirical models, npj Comput Mater 8 (2022). https://doi.org/10.1038/s41524-022-00768-w.

[6] P. Erhart, K. Albe, Analytical potential for atomistic simulations of silicon, carbon, and silicon carbide, Phys. Rev. B 71 (2005). https://doi.org/10.1103/PhysRevB.71.035211.

[7] M. Zieglowski, S. Trosien, J. Rohrer, S. Mehlhase, S. Weber, K. Bartels, G. Siegert, T. Trellenkamp, K. Albe, M. Biesalski, Reactivity of Isocyanate-Functionalized Lignins: A Key Factor for the Preparation of Lignin-Based Polyurethanes, Front. Chem. 7 (2019) 562. https://doi.org/10.3389/fchem.2019.00562.

[8] P.E. Blöchl, Projector augmented-wave method, Phys. Rev. B 50 (1994) 17953–17979.

[9] G. Kresse, J. Furthmüller, Efficient iterative schemes for ab initio total-energy calculations using a plane-wave basis set, Phys. Rev. B 54 (1996) 11169–11186.

[10] A. Hjorth Larsen, J. Jørgen Mortensen, J. Blomqvist, I.E. Castelli, R. Christensen, M. Dułak, J. Friis, M.N. Groves, B. Hammer, C. Hargus, E.D. Hermes, P.C. Jennings, P. Bjerre Jensen, J. Kermode, J.R. Kitchin, E. Leonhard Kolsbjerg, J. Kubal, K. Kaasbjerg, S. Lysgaard, J. Bergmann Maronsson, T. Maxson, T. Olsen, L. Pastewka, A. Peterson, C. Rostgaard, J. Schiøtz, O. Schütt, M. Strange, K.S. Thygesen, T. Vegge, L. Vilhelmsen, M. Walter, Z. Zeng, K.W. Jacobsen, The atomic simulation environment-a Python library for working with atoms, J. Phys. Condens. Matter 29 (2017) 273002. https://doi.org/10.1088/1361-648X/aa680e.

[11] J. Enkovaara, C. Rostgaard, J.J. Mortensen, J. Chen, M. Dułak, L. Ferrighi, J. Gavnholt, C. Glinsvad, V. Haikola, H.A. Hansen, H.H. Kristoffersen, M. Kuisma, A.H. Larsen, L. Lehtovaara, M. Ljungberg, O. Lopez-Acevedo, P.G. Moses, J. Ojanen, T. Olsen, V. Petzold, N.A. Romero, J. Stausholm-Møller, M. Strange, G.A. Tritsaris, M. Vanin, M. Walter, B. Hammer, H. Häkkinen, G.K.H. Madsen, R.M. Nieminen, J.K. Nørskov, M. Puska, T.T. Rantala, J. Schiøtz, K.S. Thygesen, K.W. Jacobsen, Electronic

structure calculations with GPAW: a real-space implementation of the projector augmented-wave method, J. Phys. Condens. Matter 22 (2010) 253202. https://doi.org/10.1088/0953-8984/22/25/253202.
[12] J.P. Perdew, K. Burke, M. Ernzerhof, Generalized Gradient Approximation Made Simple, Phys. Rev. Lett. 77 (1996) 3865–3868.
[13] H.J. Monkhorst, J.D. Pack, Special points for Brillouin-zone integrations, Phys. Rev. B 13 (1976) 5188–5192.